# Flat Optical Frequency Comb Generator Based on Integrated Lithium Niobate Modulators

Mengyue Xu, Mingbo He, Yuntao Zhu, Siyuan Yu, and Xinlun Cai

*(Invited Paper)*

***Abstract*—Chip-scale electro-optic (EO) frequency combs are expected to play an essential role in future high-capacity optical communications systems and next-generation mobile communications. The application requires integrated EO frequency comb generators featuring good spectral flatness, high modulation bandwidth, low driving voltage and low insertion loss simultaneously. Here, we demonstrate a flat-top optical flat comb (OFC) generator based on high-performance lithium niobate on insulator modulators. The OFC generator shows a low on-chip loss (2.1 dB), a low driving voltage over a broad frequency range, and a large 3-dB EO bandwidth. Moreover, with consuming power of less than 2W, the presented device produces 13 lines with a power variation of less than 1.2 dB and a line spacing of 31 GHz which can further be extended to 67 GHz.**

***Index Terms*—Electrooptic modulation, lithium niobate on insulator, Microwave photonics, nanophotonics, optical frequency comb, optical waveguides.**

## I. Introduction

A FREQUENCY comb is a multi-wavelength laser source with coherent and evenly-spaced frequency lines. In recent decades, applications of optical frequency combs (OFCs) have rapidly grown across diverse fields of metrology [1], spectroscopy [2], atomic clock [3], optical communication [4] and microwave photonics [5]. Particularly, OFCs can be used to efficiently generate terahertz waves which are expected to play an important role in future 6G mobile communications [6], [7]. Various on-chip frequency comb generators schemes, including mode-locked lasers (MLLs) [8], microresonator-based Kerr frequency comb [9], [10] and electro-optic (EO) frequency combs [11], [12], have different characteristics suitable for specified applications. Modern communication systems require OFCs with a compact size, spectral flatness, narrow optical linewidth, higher per comb line power [4]. An attractive solution to achieve these demands is EO frequency combs. Moreover, the EO frequency comb enjoys an extraordinary degree of freedom of continuously tuning line spacing and central frequency. These features are highly desirable especially for dense wavelength division multiplexing (DWDM) sources in optics fiber communications applications.

In a conventional EO frequency comb generator, the continuous-wave laser is injected into cascaded commercial-off-the-shelf lithium niobate (LN) modulators [13]–[16], which have demonstrated spectral stability, flexible line spacing and a relatively good spectral flatness. However, these OFC generation schemes are generally composed of several discrete optical components resulting in bulky size and high cost. Moreover, the generated combs have limited power per line due to the high insertion optical loss ($\sim$ 4-5 dB loss per modulator). Indeed, when these OFCs are used for generating tens of light sources in a coherent DWDM system, the limited power per line will compromise the optical signal-to-noise ratio (OSNR) and degrade transmission performance. [4], [17].

On-chip EO comb generation has been demonstrated on silicon-on-insulator [11], [18] and InP [19]. However, both of them suffer from large insertion loss and nonlinear phase modulation [20]. LN material enjoys a strong linear EO effect, high intrinsic modulation bandwidth and wide optical transparency window [21], [22] and the emerging lithium niobate on insulator (LNOI) platform brings the performance to a new level. The LNOI-based modulators can achieve ultra-low optical loss ($\sim$3 dB/m) [23], high modulation bandwidth and low RF driving voltage simultaneously [24]–[29]. These advantages enable high power per comb line, tunable range of line spacing and lower energy consumption for EO comb generation. Moreover, the LNOI platform is highly promising for future large-scale multi-functional photonic integrated circuits (PICs). [30]

In this paper, we demonstrate the generation of a flat-top OFC by integrating a push-pull Mach-Zehnder modulator (MZM) and a phase modulator (PM) in LNOI platform. Note that the work reported here extends our preliminary results [31] by adding detailed simulations and additional experimental results. The EO comb generator features a low on-chip loss of 2.1 dB. By applying a driving RF signal of $\sim$1.8 W to the PM with a low

Manuscript received May 31, 2021; revised July 13, 2021; accepted July 23, 2021. Date of publication July 27, 2021; date of current version January 16, 2022. This work was supported in part by the National Key R&D Program of China under Grants 2019YFA0705000 and 2019YFB1803900, in part by the National Natural Science Foundation of China under Grants 11690031 and 11761131001, in part by the Key R&D Program of Guangdong Province under Grant 2018B030329001, in part by the Local Innovative and Research Teams Project of Guangdong Pearl River Talents Program under Grant 2017BT01X121, in part by the Innovation Fund of WNLO under Grant 2018WNLOKF010, and in part by the Project of Key Laboratory of Radar Imaging and Microwave Photonics, Ministry of Education under Grant RIMP2019003. *(Corresponding author: Xinlun Cai.)*

The authors are with the State Key Laboratory of Optoelectronic Materials and Technologies, and School of Electronics and Information Technology, Sun Yat-sen University, Guangzhou 510000, China (e-mail: xumy26@mail2.sysu.edu.cn; hemingb@mail2.sysu.edu.cn; zhuyt59@mail.sysu.edu.cn; yusy@mail.sysu.edu.cn; caixlun5@mail.sysu.edu.cn).

Color versions of one or more figures in this article are available at https://doi.org/10.1109/JLT.2021.3100254.

Digital Object Identifier 10.1109/JLT.2021.3100254

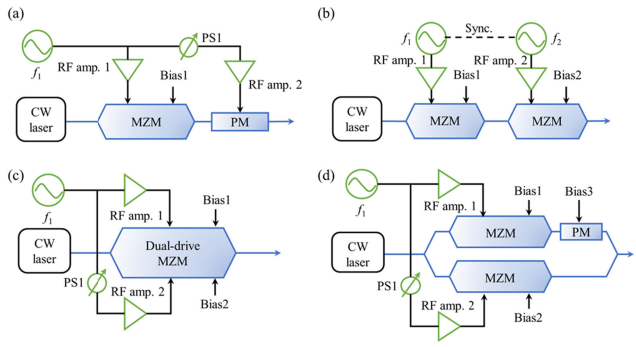


Fig. 1. Diagram of flat comb generator based on (a) cascaded MZM and PM, [32], [33] (b) cascaded MZMs [11], (c) dual-drive MZM [16], [34], and (d) in-phase and quadrature (IQ) modulators. [18].

half-wave voltage, we obtained 13 comb lines with a spacing of 31 GHz (corresponding to spectral bandwidths up to 403 GHz), and a spectral power variation of less than 1.2 dB. Moreover, the device demonstrates broadband operation in the C band and the line spacing range can be further extended from 30 GHz to more than 60 GHz due to the large modulation bandwidths of $>$ 67 GHz.

## II. Device Design and Fabrication

Several EO schemes for generating flat optical combs have been demonstrated so far, including cascaded MZM or PM [11], [32], [33], dual-drive MZM [16], [34] and in-phase and quadrature (IQ) modulators [18], as shown in Fig. 1. Among them, the scheme of cascading a MZM and a PM features the simplest external control circuit, as it requires only a DC bias voltage and an RF driving signal (Fig. 1(a)). To date, this scheme has only been implemented in bulky discrete optical components, which are not only cumbersome to use, but also difficult to ensure a stable phase relationship between the MZM and PM. In this work, we demonstrated an integrated circuit consisting of one MZM and one PM for generating flat OFCs.

Fig. 2(a) and (b) shows the schematic of the integrated EO comb generator and a microscope image of the fabricated device. The balanced MZM is driven in a single-drive series push-pull mode. We adopt 3dB 1 $\times$ 2 multimode interference (MMI) couplers to split and combine the light in the MZM. Both PM and MZM adopt highly-confined etched LN waveguides and optimized traveling-wave electrodes (TWE) for reducing driving voltage and high-speed modulation. Two parallel TWEs are placed side by side and arranged in ground-signal-ground-signal-ground (GSGSG) configuration for a compact arrangement. In this manner, both MZM and PM are operated in a traveling-wave modulation because the light waves always co-propagate with modulating microwaves.

Fig. 2. (c) illustrated the schematic of a cross-section of the MZM. The designed waveguides have a top width of $w_{\mathrm{LN}} = 4\ \mu$m, a slab thickness of $t_{\mathrm{s}} = 300$ nm and a rib height of $t_{\mathrm{r}} = 300$ nm. We optimized the width of the signal electrode ($w_{\mathrm{s}} = 17\ \mu$m) and the thickness of electrodes ($t = 0.9\ \mu$m) to achieve 50-ohm impedance matching. The electrode spacing $w_{\mathrm{g}}$ was set to 7 $\mu$m to achieve a good balance between optical loss (simulated optical loss $\sim$0.04 dB/cm), microwave propagation loss and modulation efficiency (2.6 Vcm). The above parameters are adopted for both modulators. We also present the calculated $\mathrm{TE}_0$ mode distribution for the LN ridge waveguide in Fig. 2. (c), which illustrates good optical confinement. Fig. 2. (d) shows the electric field distribution when a direct current voltage of 10 V is applied across the electrodes. The majority of the electric field is concentrated between the electrodes gap, thus induce an effective refractive change of the optical mode. Longer modulation section results in lower $V_\pi$ but larger RF losses. In this work, each modulator has a modulation length of 14 mm to balanced RF $V_\pi$ and modulation bandwidth.

We fabricated the present device on a commercially-available X-cut LNOI wafer (NANOLN) consisting of a 600 nm LN film on a 2.5 $\mu$m $SiO_2$/Si substrate. Firstly, we used electron-beam lithography (EBL) and dry etching process to define the optical waveguide patterns of the present device in the LNOI wafer. Next, we fabricated amorphous-Si/LN vertical grating couplers for off-chip coupling, which were designed for transverse-electric (TE) mode operation over the C band [35]. Finally, we patterned 900-nm-thick gold traveling-wave electrodes through a lift-off process. More fabrication details are described in our previous work [36]. The total size of the device is 15 mm $\times$ 0.5 mm, which is much smaller than the commercial counterparts (at least$\sim$ 100 mm $\times$ 10 mm).

## III. Experiments and Results

### A. Characterization of Modulators

The total insertion loss of the device at peak transmission is measured to be 8.9 dB. The coupling loss of the grating coupler is $\sim$ 3.4 dB per facet. Therefore, the on-chip insertion loss is estimated to be 2.1 dB. Furthermore, the edge couplers (0.5 dB/facet [37]) can be used to replace the grating couplers to further reduce the total fiber-to-fiber loss to $\sim$3 dB. Compared with the OFC generator with discrete LN modulators, the optical loss is significantly reduced. That makes it very attractive for the practical application of the OFC in optical communication.

The high-frequency electrical response of modulators is highly related to RF $V_\pi$ and bandwidth. We use a vector network analyzer (VNA, Agilent N5227A) and a pair of 67 GHz microwave probes to characterize the electrical response. Losses of the RF cables and microwave probes are normalized by performing short-open-load-through (SOLT) standards. Fig. 3. (a) indicates that the fabricated TWEs have a good high-frequency consistency, and the 6.4-dB EE bandwidths are both $\sim$ 67 GHz. Moreover, the $S_{11}$ parameters are below -25 dB for frequencies up to 67 GHz, indicating good impedance matching, which is essential to reduce the RF power loss resulting from the reflection among the testing system, the TWEs, and the 50-$\Omega$ resistive load.

We can extract the RF loss from the measured S parameters, that value is still less than 6 dB/cm up to 50 GHz. Lower RF loss is expected to bring lower RF $V_\pi$, thus achieving a higher phase modulation index ($\Delta\theta = \pi \frac{V_p}{V_{\pi,\ \mathrm{RF}}}$, where $V_p$ is the applied voltage on PM) at a given driving RF power. The RF loss can be further decreased to $\sim$ 2 dB/cm at 50 GHz using segmented electrodes on the LN-on-quartz platform [38].

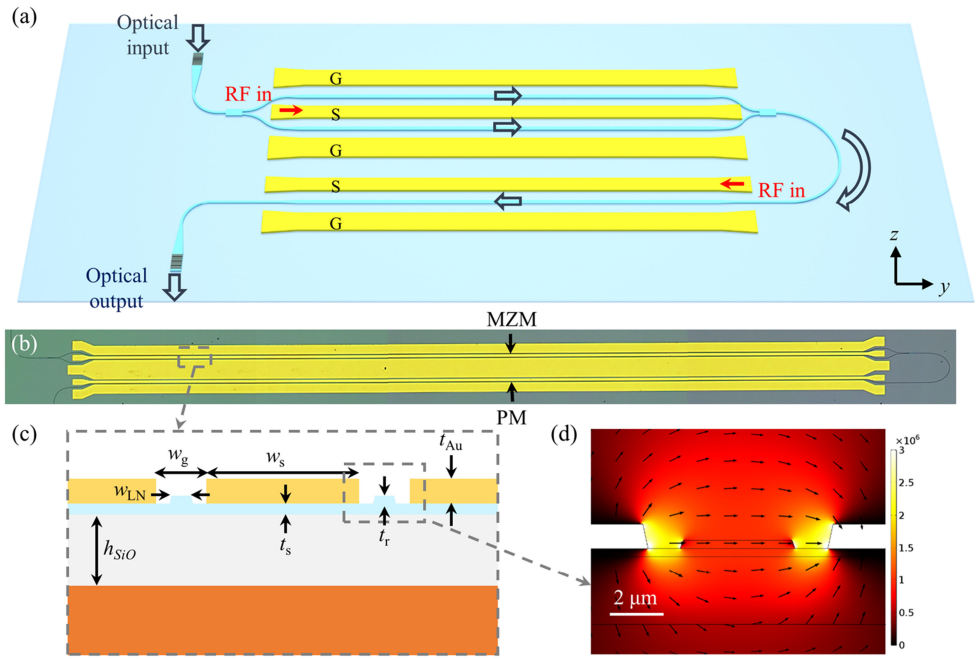


Fig. 2. (a) 3D schematic of an integrated EO frequency comb generator in LNOI platform. (b) Microscope image of the fabricated device. (c) Cross-sectional view of the EO interaction section. (d) Calculated optical TE0 mode in the etched LN waveguide.

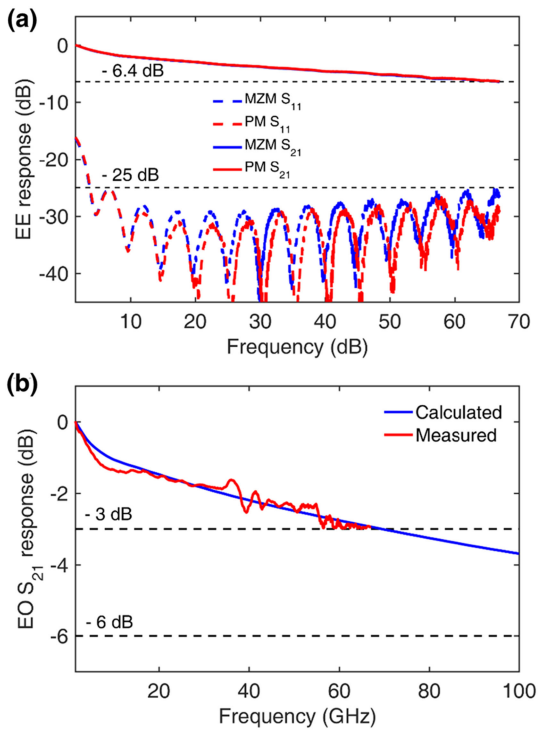


Fig. 3. (a) Measured EE S-parameters of the 14-mm PM and the MZM. (b) Measured EO S21 response (red solid line) of 14-mm MZM. The solid blue line represents the calculated result.

The upper limit on the line spacing of the EO frequency comb is dependent on the achievable EO bandwidth for the present device. We characterize the EO $S_{21}$ response of the MZM using VNA and 67-GHz photodetector (Finisar XPDV3120R). In Fig. 3(b), we observe the 3-dB EO bandwidth of 67 GHz. The calculated EO response shows a good agreement with the measured response in Fig. 3(b). Besides, a 6-dB EO bandwidth of the modulator is presumed to be over 100 GHz. The simulated model used here is described in detail in our previous work [27]. Therefore, our device is capable of producing optical frequency combs with line spacing up to 67 GHz if the measurement system does not have bandwidth limitations.

The frequency-dependent RF $V_\pi$ is the primary consideration for power efficiency. We directly measure the low-frequency $V_\pi$ of the 14-mm MZM with a 10-kHz triangular sweep, indicating a $V_\pi$ of 1.7 V in Fig. 4. (a). Note that the MZM in our device operates in push-pull mode, while the PM is modulated in a single path. Therefore, we estimate the low-frequency $V_\pi$ of PM to be $\sim 3.4$ V. Assuming perfect velocity matching between the optical wave and microwave, the RF $V_\pi$ can be predicted from the measured low-frequency $V_\pi$ and the extracted $\alpha_m$[39], [40]:

$$V_\pi\ (f) = \frac{\alpha_m\,(f)\,L}{1 - e^{-\alpha_m(f)L}}\ V_\pi\,(DC)$$

where $L$ is the length of the TWE. The calculated result is plotted in Fig. 4(b) (blue line). Meanwhile, we further confirm the RF $V_\pi$ (red circles in Fig. 4(b)) using the optical spectrum analysis method [41]. As plotted in Fig. 4. (b), the RF $V_\pi$ increases slowly from 4.3 V to 5.7 V in the frequency range of 10 GHz to 67 GHz. The value of the RF $V_\pi$ is relatively flat over a broad frequency range, which means that we can drive the PM at even higher frequencies with little compromise in the modulation index.

### *B. OFC Generation*

We use our low-RF $V_\pi$, large bandwidth, and low-loss cascaded modulators to generate flat-OFCs. Fig. 5(a) shows the experimental setup for flat OFC generations. Our device is seed by a CW laser with 13 dBm output power. A 31-GHz sinusoidal

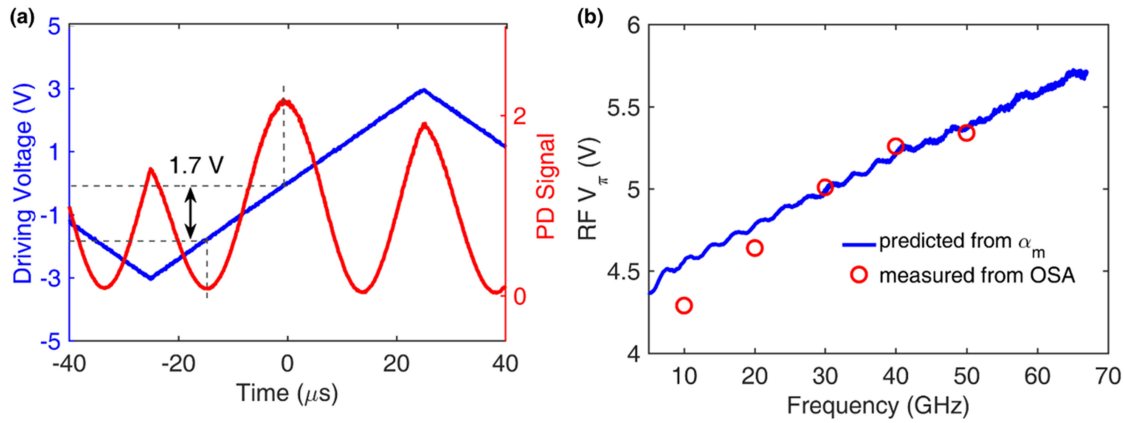


Fig. 4. (a) Low frequency modulation response of 14-mm push-pull MZM. (b) Measured RF $V_\pi$ of the 14-mm PM using spectrum analysis method (red circles) and the calculated RF $V_\pi$ predicted from the RF loss coefficient (blue line).

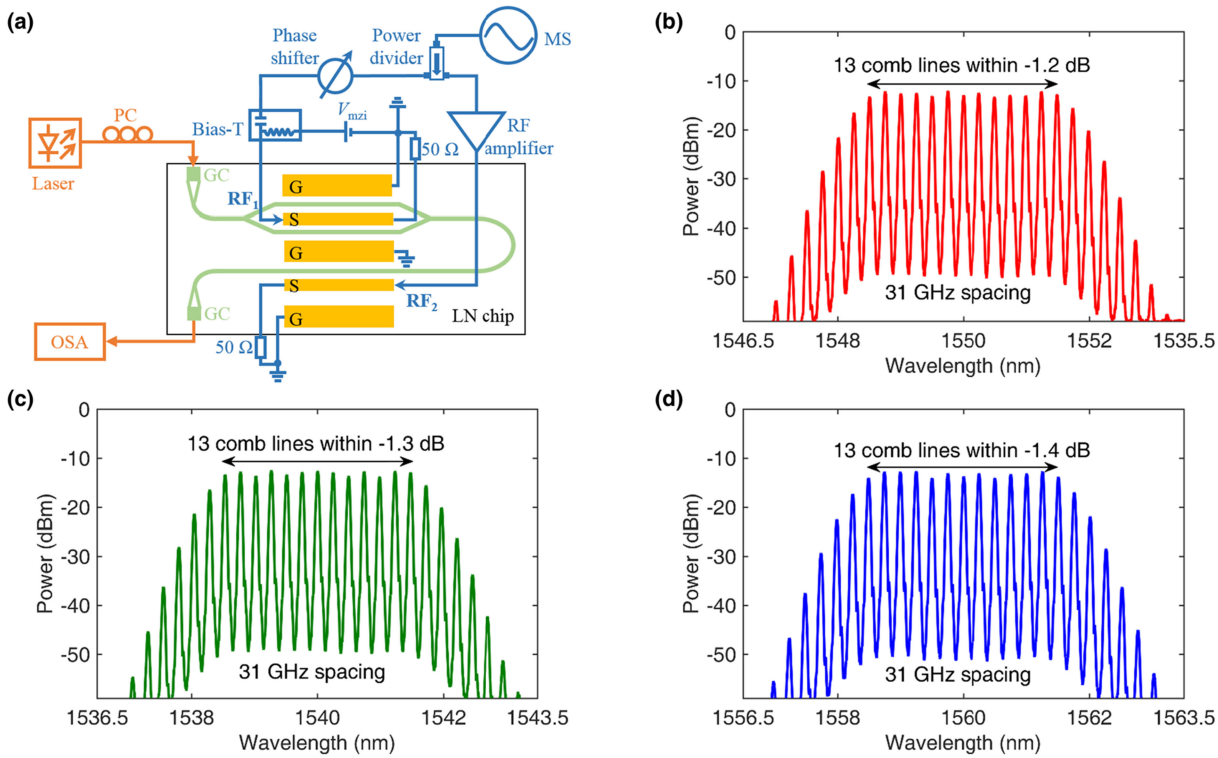


Fig. 5. (a) Experimental setup for flat OFC generation. OSA: optical spectrum analyzer, PC: polarization controller, GC: grating coupler, MS, microwave source. Measured OFC spectra at the central wavelength of (b) 1550 nm, (c) 1540 nm, and (d) 1560 nm.

signal from a microwave source (Agilent E8257D) is equally split into two by a power divider (Agilent 11636C). One of the RF signals ($RF_1$) is sent to the MZM, and we can obtain the optimum flatness when the amplitude of the $RF_1$ is 0.5 $V_\pi$ and the bias point is $0.35V_\pi$ [33]. The other RF signal ($RF_2$) reaches the PM after being amplified by a high-gain power amplifier for achieving a high modulation index. Taking into account the losses of RF cable and probe, the actual RF power applied to the PM is about 1.8 W, with a corresponding phase modulation index of 8.4. The RF signals are coupled to the microwave electrode through a pair of GSGSG configured probes, and are terminated by a pair of 50 Ω loads. An RF phase shifter is used to synchronize the parabolic-like pulse with the sinusoidal phase modulation in the time domain. Finally, we monitor the output optical signal by an optical spectrum analyzer (OSA, Anritsu MS9740A) with a minimum resolution of 0.03 nm.

Fig. 5(b) presents 13 comb lines with a line spacing of 31 GHz, which has a power variation within 1.2 dB, and a central wavelength of 1550 nm. To demonstrate the multi-wavelength operation, we tune the input laser at the wavelength of 1540 nm and 1560 nm. We find that all the generated comb lines at different operating wavelengths have similar properties (flatness, number of generated lines). Besides, the OFC spectra in

TABLE I
COMPARISON OF SEVERAL PERFORMANCE METRICS FOR FLAT EO COMB GENERATORS

| Symbol | Loss (dB) | Number of lines | Flatness (dB) | Maximum line spacing (GHz) | Total spectral bandwidth (GHz) |
|---|---|---|---|---|---|
| This work | 2.1 | 13 | 1.2 | 31 | 403 |
| Silicon [42] | N.A. | 15 | 6 | 5 | 75 |
| Silicon [18] | 14.1 | 5 | 2.1 | 10 | 50 |
| Silicon [11] | 13[a] | 9 | 6.5 | 10 | 90 |
| Silicon [34] | 6.5 | 5 | 0.6 | 20 | 100 |
| Commercial LN [14] | 11[b] | 60 | 10 | 18 | 1080 |
| Commercial LN [16] | N.A. | 11 | < 1 | 6 | 66 |
| Commercial LN [43] | 5~7 dB | 16 | 0.3 | 20 | 320 |
| InP [20, 44] | 6[c] | 9 | 0.77 | 12.5 | 112.5 |

[a]This value was calculated from 24 dB fiber-to-fiber insertion loss and 11 dB coupling loss.
[b]This value was calculated from 3 dB for each PM (3 PMs used) and 2 dB for the IM.
[c]This value was calculated from 13 dB fiber-to-fiber insertion loss and 3.5 dB/facet coupling loss.

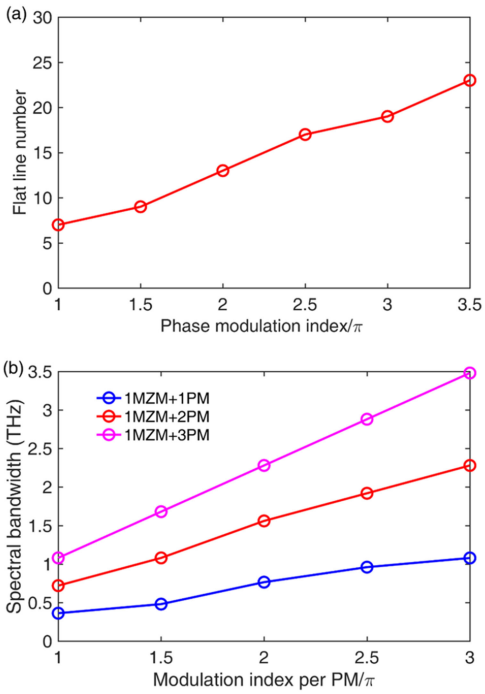


Fig. 6. (a) Calculated phase modulation index as a function of the number of comb lines within 3dB spectral power variation. (b) Calculated phase modulation index for per PM as a function of the spectral bandwidth within 3dB spectral power variation. The relationships are displayed for cascaded a MZM with one, two and three PMs, respectively. Assuming the frequency spacing is 60 GHz.

Fig. 5 features a power contrast of over 45 dB between the comb and the background noise.

Concerning the number of flat comb lines, it determines by the phase modulation index ($\Delta\theta$). In Fig. 6. (a), we calculate its relationship to the phase modulation index ($\Delta\theta$). In terms of the demonstrated device, we can further increase the amplitude of the RF signal on the phase modulator within the average power-handling capability. To increase power efficiency, we need to optimize PM to achieve a low $V_\pi$ in high frequency. As the simulation is shown in Fig. 6. (b), 1-Thz flat spectral bandwidth can be realized by a modulation index of $3\pi$, $1.5\pi$ and $\pi$ on each of one, two and three PMs, respectively. It can be seen that the total power consumption on PMs is the same to achieve the same spectral bandwidth, but more PMs mean a greater number of microwave amplifiers.

## IV. DISCUSSION AND CONCLUSION

In Table I, we compare the performance of our on-chip device with flat-OFC generators based on other material platforms, including silicon, commercial LN, and InP. Both silicon and InP based devices rely on modulating mechanisms which are intrinsically nonlinear and lossy (carrier dispersion effect and quantum-confinement Stark effect respectively). Therefore, special care must be taken with Si- and InP-based devices to achieve a good flatness [20], while LN-based devices can provide linear and pure phase modulation. By cascading discrete commercial LN modulators, one can obtain a broad and flat OFC, but the total insertion loss is still relatively high, and the maximum line spacing is limited around 35 GHz due to the bandwidth limitations in conventional LN modulators. The presented OFC generator features the lowest insertion loss and highest reported line spacing.

In conclusion, we have demonstrated an on-chip flat-top comb generator on the LNOI platform. The presented OFC generator made up of cascading a MZM and a PM, featuring a low on-chip optical loss, low RF $V_\pi$ (4.3V at 10 GHz for a PM), and large EO bandwidth (~67 GHz). We obtain the 13 lines OFC

with a line spacing of 31 GHz and demonstrate the wavelength-tunable in the C band with good spectral smoothness (variations $<$1.4 dB). The demonstrated OFC device is very attractive for a high-capacity transmission system, because the sidebands from our device are well suited for loading high baud rate signals. Moreover, the low optical loss also allows us to cascade more PMs to broaden the spectral bandwidth without significantly decrease power per comb line.

## REFERENCES


[1] T. Udem, R. Holzwarth, and T. W. Hänsch, "Optical frequency metrology," *Nature,* vol. 416, no. 6877, pp. 233–237, 2002.

[2] N. Picqué and T. W. Hänsch, "Frequency comb spectroscopy," *Nature Photon.,* vol. 13, no. 3, pp. 146–157, 2019.

[3] Z. L. Newman *et al.*, "Architecture for the photonic integration of an optical atomic clock," *Optica,* vol. 6, no. 5, pp. 680–685, 2019.

[4] V. Torres-Company *et al.*, "Laser frequency combs for coherent optical communications," *J. Lightw. Technol.,* vol. 37, no. 7, pp. 1663–1670, 2019.

[5] V. Torres-Company and A. M. Weiner, "Optical frequency comb technology for ultra-broadband radio-frequency photonics," *Laser Photon. Rev.,* vol. 8, no. 3, pp. 368–393, 2014.

[6] G. K. M. Hasanuzzaman, A. Kanno, P. T. Dat, and S. Iezekiel, "Self-Oscillating optical frequency comb: Application to low phase noise millimeter wave generation and radio-over-fiber link," *J. Lightw. Technol.,* vol. 36, no. 19, pp. 4535–4542, 2018.

[7] C. Browning *et al.*, "Gain-switched optical frequency combs for future mobile radio-over-fiber millimeter-wave systems," *J. Lightw. Technol.,* vol. 36, no. 19, pp. 4602–4610, 2018.

[8] Z. Wang *et al.*, "A III-V-on-Si ultra-dense comb laser," *Light: Sci. Appl.,* vol. 6, no. 5, pp. e16260–e16260, 2017.

[9] X. Xue, P.-H. Wang, Y. Xuan, M. Qi, and A. M. Weiner, "Microresonator Kerr frequency combs with high conversion efficiency," *Laser Photon. Rev.,* vol. 11, no. 1, 2017, Art. no. 1600276.

[10] X. Xue, X. Zheng, and B. Zhou, "Super-efficient temporal solitons in mutually coupled optical cavities," *Nature Photon.,* vol. 13, no. 9, pp. 616–622, 2019.

[11] Z. Wang *et al.*, "Optical frequency comb generation using CMOS compatible cascaded mach–zehnder modulators," *IEEE J. Quantum Electron.,* vol. 55, no. 6, pp. 1–6, Dec. 2019.

[12] A. Parriaux, K. Hammani, and G. Millot, "Electro-optic frequency combs," *Adv. Opt. Photon.,* vol. 12, no. 1, pp. 223–287, 2020.

[13] R. Wu, V. R. Supradeepa, C. M. Long, D. E. Leaird, and A. M. Weiner, "Generation of very flat optical frequency combs from continuous-wave lasers using cascaded intensity and phase modulators driven by tailored radio frequency waveforms," *Opt. Lett.,* vol. 35, no. 19, pp. 3234–3236, 2010.

[14] A. J. Metcalf, V. Torres-Company, D. E. Leaird, and A. M. Weiner, "High-Power broadly tunable electrooptic frequency comb generator," *IEEE J. Sel. Topics Quantum Electron.,* vol. 19, no. 6, pp. 231–236, Nov./Dec. 2013.

[15] T. Lin, S. Zhao, Z. Zhu, X. Li, and K. Qu, "Generation of flat optical frequency comb based on a DP-QPSK modulator," *IEEE Photon. Technol. Lett.,* vol. 29, no. 1, pp. 146–149, Jan. 2017.

[16] N. Yokota, K. Abe, S. Mieda, and H. Yasaka, "Harmonic superposition for tailored optical frequency comb generation by a Mach–Zehnder modulator," *Opt. Lett.,* vol. 41, no. 5, pp. 1026–1029, 2016.

[17] H. Hu and L. K. Oxenløwe, "Chip-based optical frequency combs for high-capacity optical communications," *Nanophotonics*, vol. 10, no. 5, pp. 1367–1385, 2021.

[18] S. Liu *et al.*, "Microwave pulse generation with a silicon dual-parallel modulator," *J. Lightw. Technol.,* vol. 38, no. 8, pp. 2134–2143, 2020.

[19] F. Bontempi, N. Andriolli, F. Scotti, M. Chiesa, and G. Contestabile, "Comb line multiplication in an InP integrated photonic circuit based on cascaded modulators," *IEEE J. Sel. Topics Quantum Electron.,* vol. 25, no. 6, pp. 1–7, 2019.

[20] N. Yokota and H. Yasaka, "Operation strategy of InP Mach–Zehnder modulators for flat optical frequency comb generation," *IEEE J. Quantum Electron.,* vol. 52, no. 8, pp. 1–7, Aug. 2016.

[21] A. Rao and S. Fathpour, "Compact lithium niobate electrooptic modulators," *IEEE J. Sel. Topics Quantum Electron.*, vol. 24, no. 4, pp. 1–14, Jul./Aug. 2018.

[22] A. Boes, B. Corcoran, L. Chang, J. Bowers, and A. Mitchell, "Status and potential of lithium niobate on insulator (LNOI) for photonic integrated circuits," *Laser Photon. Rev.,* vol. 12, no. 4, pp. 1700 256-1–1700 256-19, Apr. 2018.

[23] M. Zhang, C. Wang, R. Cheng, A. Shams-Ansari, and M. Lončar, "Monolithic ultra-high-Q lithium niobate microring resonator," *Optica,* vol. 4, no. 12, pp. 1536–1537, 2017.

[24] C. Wang *et al.*, "Integrated lithium niobate electro-optic modulators operating at CMOS-compatible voltages," *Nature,* vol. 562, no. 7725, pp. 101–104, 2018.

[25] T. Ren *et al.*, "An integrated low-voltage broadband lithium niobate phase modulator," *IEEE Photon. Technol. Lett.,* vol. 31, no. 11, pp. 889–892, Jun. 2019.

[26] M. He *et al.*, "High-performance hybrid silicon and lithium niobate Mach–Zehnder modulators for 100 Gbit s$-$1 and beyond," *Nature Photon.,* vol. 13, pp. 359–364, 2019.

[27] M. Xu *et al.*, "High-performance coherent optical modulators based on thin-film lithium niobate platform," *Nature Commun.,* vol. 11, no. 1, p. 3911-1–3911-7, 2020.

[28] M. Xu *et al.*, "Michelson interferometer modulator based on hybrid silicon and lithium niobate platform," *APL Photon.,* vol. 4, no. 10,2019, Art. no. 100802.

[29] X. Wang, P. O. Weigel, J. Zhao, M. Ruesing, and S. Mookherjea, "Achieving beyond-100-GHz large-signal modulation bandwidth in hybrid silicon photonics Mach-Zehnder modulators using thin film lithium niobate," *APL Photon.,* vol. 4, no. 9, 2019, Art. no. 096101.

[30] K. Luke, P. Kharel, C. Reimer, L. He, M. Loncar, and M. Zhang, "Wafer-scale low-loss lithium niobate photonic integrated circuits," *Opt. Exp.,* vol. 28, no. 17, pp. 24452–24458, 2020.

[31] M. Xu, M. He, and X. Cai, "Generation of flat optical frequency comb using integrated cascaded lithium niobate modulators," in *Conf. Lasers Electro-Opt.*, WA, DC, USA, 2020, pp. STh1O.5-1–STh1O.5-2.

[32] Y. Dou, H. Zhang, and M. Yao, "Generation of flat optical-frequency comb using cascaded intensity and phase modulators," *IEEE Photon. Technol. Lett.,* vol. 24, no. 9, pp. 727–729, May 2012.

[33] Y. Dou, H. Zhang, and M. Yao, "Improvement of flatness of optical frequency comb based on nonlinear effect of intensity modulator," *Opt. Lett.,* vol. 36, no. 14, pp. 2749–2751, 2011.

[34] J. Lin, H. Sepehrian, Y. Xu, L. A. Rusch, and W. Shi, "Frequency comb generation using a CMOS compatible SiP DD-MZM for flexible networks," *IEEE Photon. Technol. Lett.,* vol. 30, no. 17, pp. 1495–1498, Sep. 2018.

[35] J. Jian *et al.*, "High-efficiency hybrid amorphous silicon grating couplers for sub-micron-sized lithium niobate waveguides," *Opt. Exp.,* vol. 26, no. 23, pp. 29651–29658, 2018.

[36] J. Jian *et al.*, "High modulation efficiency lithium niobate Michelson interferometer modulator," *Opt. Exp.,* vol. 27, no. 13, pp. 18731–18739, 2019.

[37] P. Ying *et al.*, "Low-loss edge-coupling thin-film lithium niobate modulator with an efficient phase shifter," *Opt. Lett.,* vol. 46, no. 6, pp. 1478–1481, 2021.

[38] P. Kharel, C. Reimer, K. Luke, L. He, and M. Zhang, "Breaking voltage–bandwidth limits in integrated lithium niobate modulators using micro-structured electrodes," *Optica,* vol. 8, no. 3, pp. 357–363, 2021.

[39] E. I. Ackerman *et al.*, "RF-Over-Fiber links with very low noise figure," *J. Lightw. Technol.,* vol. 26, no. 15, pp. 2441–2448, 2008.

[40] A. Chen and E. Murphy, *Broadband Optical Modulators*. Boca Raton, FL, USA: CRCPress, 2011.

[41] S. Yongqiang, Y. Lianshan, and A. E. Willner, "High-speed electrooptic modulator characterization using optical spectrum analysis," *J. Lightw. Technol.,* vol. 21, no. 10, pp. 2358–2367, 2003.

[42] S. Liu, K. Wu, L. Zhou, X. Xiao, Y. Zhong, and J. Chen, "Optical frequency comb generation and microwave synthesis with integrated cascaded silicon modulators," in *Proc. Conf. Lasers Electro-Opt.*, San Jose, CA, USA, 2018, p. JW2A.56-1–JW2A.562.

[43] K. Qu, S. Zhao, X. Li, Z. Zhu, D. Liang, and D. Liang, "Ultra-flat and broadband optical frequency comb generator via a single Mach–Zehnder modulator," *IEEE Photon. Technol. Lett.,* vol. 29, no. 2, pp. 255–258, Jan. 2017.

[44] N. Kikuchi *et al.*, "80-Gb/s Low-Driving-Voltage InP DQPSK modulator with an n-p-i-n structure," *IEEE Photon. Technol. Lett.,* vol. 21, no. 12, pp. 787–789, Jun. 2009.

**Mengyue Xu** received the B.S. degree in material science from Shanghai University, Shanghai, China, in 2017. She is currently working toward the Ph.D. degree with the School of Electronics and Information Technology, Sun Yat-sen University, Guangzhou, China. Her current research interests include optical communication and photonic integrated devices.

**Mingbo He** received the master's degree in microelectronics and solid state electronics from Sun Yat-sen University, Guangzhou, China, in 2018. He is currently working toward the Ph.D. degree in microelectronics and solid state electronics, Sun Yat-sen University, Guangzhou, China. His research focuses on integrated lithium niobate devices.

**Yuntao Zhu** received the master's degree in optical engineering from South China Normal University, Guanzhou, China, in 2015 and the Ph.D. degree in optics from Sun Yat-sen University, Guangzhou, China, in 2021. He is currently a Postdoctoral Research Fellow with Sun Yat-sen University. His current research focuses on hybrid integrated optical chips.

**Siyuan Yu** received the bachelor's degree in wireless technologies from Tsinghua University, Beijing, China, in 1984, the master's degree in optical communications from the Wuhan Research Institute of Post and Telecommunications, Wuhan, China, in 1987, and the Ph.D. degree in photonics from the University of Glasgow, Glasgow, U.K., in 1997. He is currently a Professor of photonic information systems with the University of Bristol, Bristol, U.K., and also a Special Expert Professor with Sun Yat-sen University, Guangzhou, China. His research interests include photonic devices, photonic integrated circuits, and their applications in optical communication systems.

**Xinlun Cai** received the Ph.D. degree in electrical and electronics engineering from the University of Bristol, Bristol, U.K., in 2012. He is currently a Professor with the School of Electronics and Information Technology, Sun Yat-sen University, Guangzhou, China. His research mainly focuses on optical communication and photonic integrated devices.